Supporting Information

Evolution of PtCu Tripod Nanocrystals to Dendritic Triangular Nanocrystals and Study of the Electrochemical Performance of Alcohol Electrooxidation

Houkang Pu[1,†], Te Zhang[1,†], Kaiyu Dong[1], Huizhen Dai[1], Luming Zhou[1], Kuankuan Wang[1], Shuxing Bai[1], Yingying Wang[2,*], Yujia Deng[1,*]

1. School of Chemistry and Chemical Engineering, Qingdao University, Ningxia Road 308, Qingdao 266071, China
2. Qingdao Hengxing University of Science and Technology, Jiushui East Road 588, Qingdao 266100, China

* Correspondence: wangyy_hx@163.com (Y. Wang); dengyujia@qdu.edu.cn (Y. Deng)

† These authors contributed equally to this work.

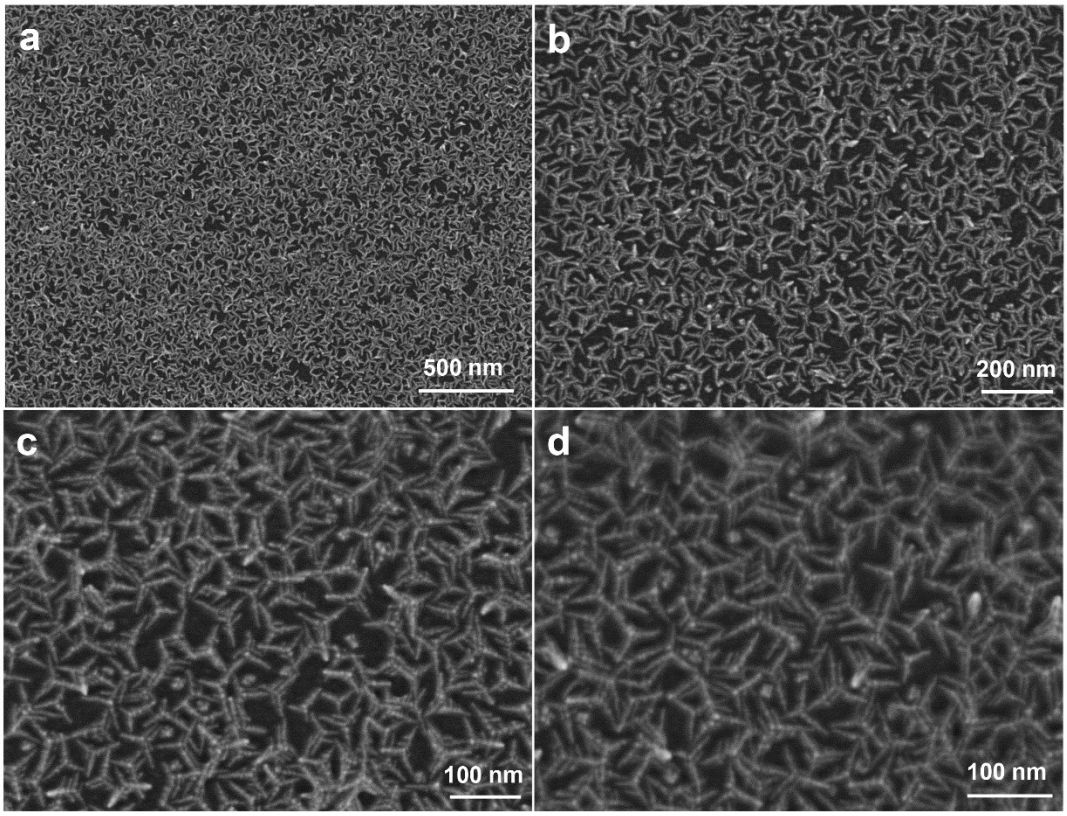

Figure S1. SEM images of TDNs at different magnifications

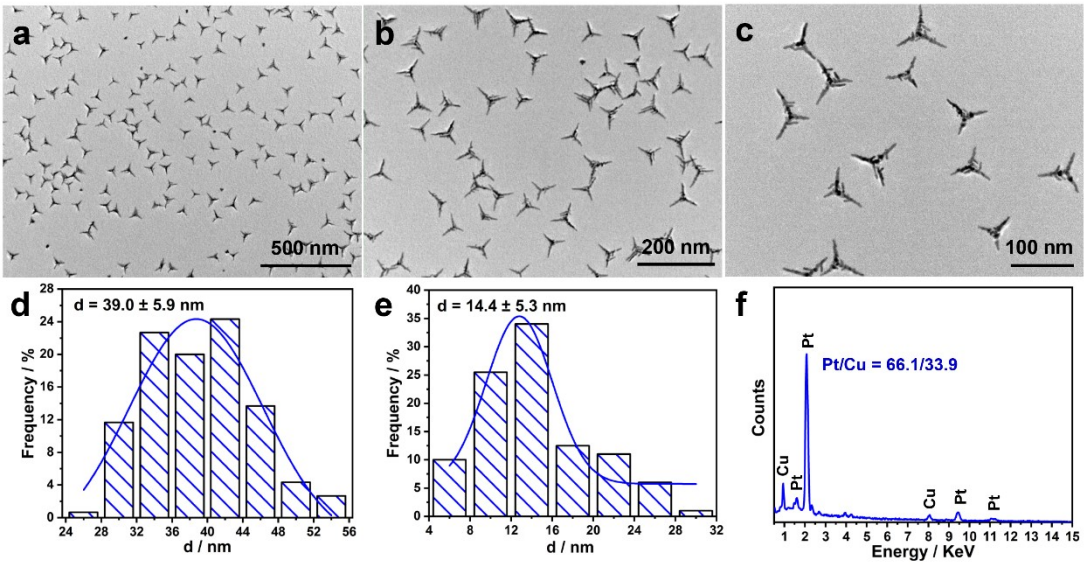

Figure S2. (a)−(c) TEM image of TDNs. (d) and (e) Histogram of the length distributions of the main branches and secondary branches of TNDs. (f) SEM−EDS spectrum of TNDs.

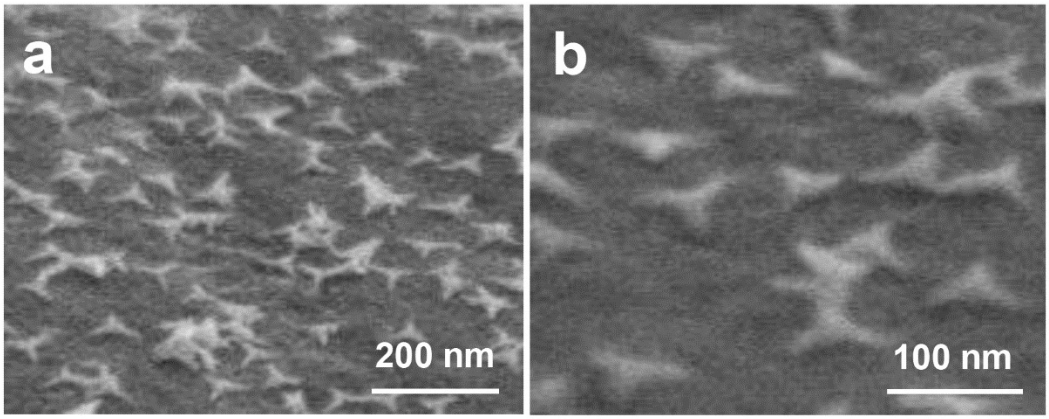

Figure S3. (a) and (b) SEM images of that TNDs were placed on a substrate at a 45° tilt and rotated 15° in the SEM (i.e. rotated by 60°).

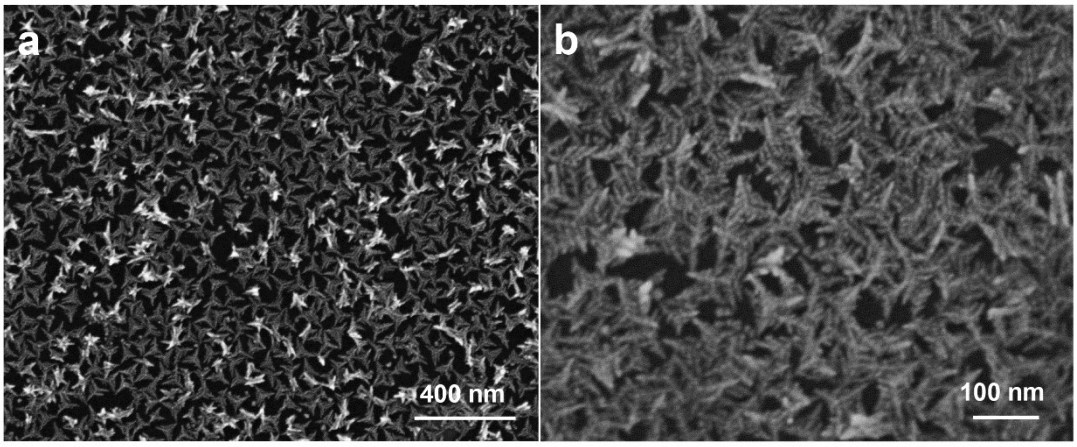

Figure S4. SEM images of PtCu TNDs obtained with standard procedures under different NaI content: (a) 200 and (b) 250 mg.

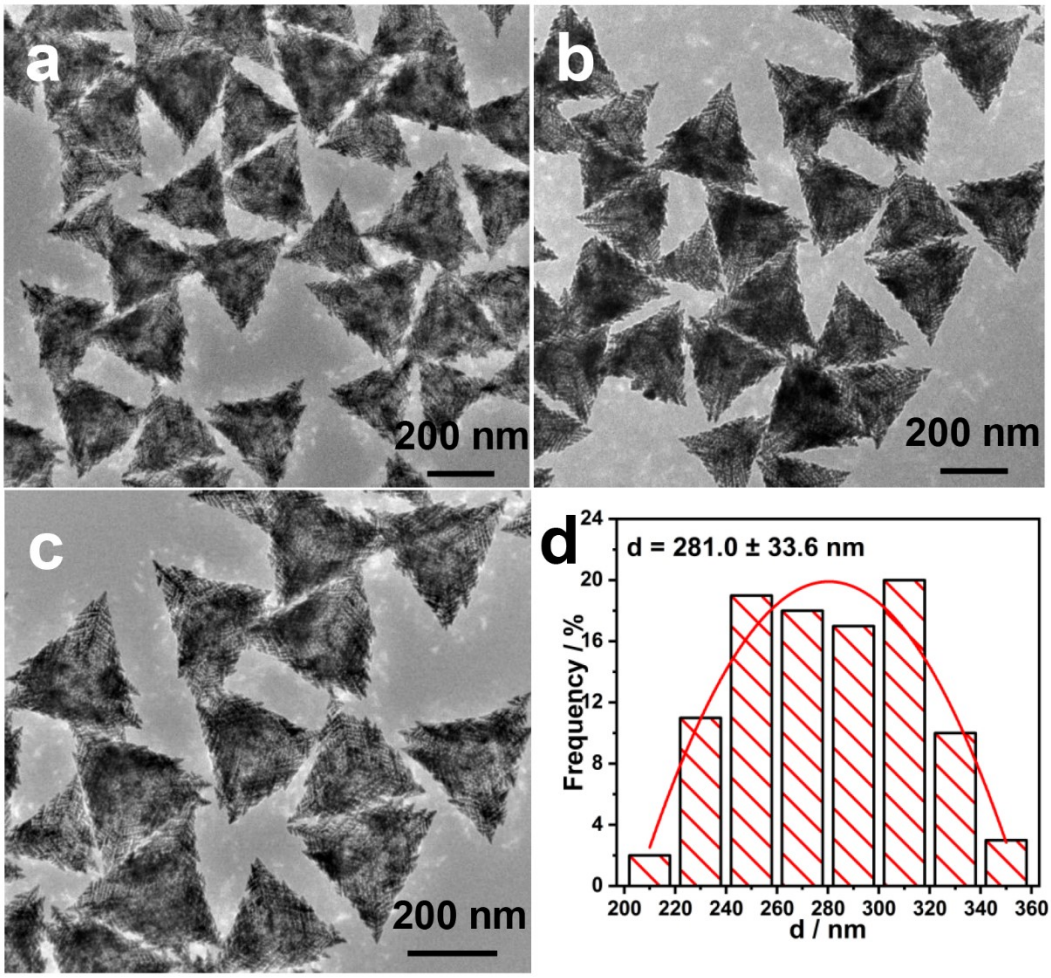

Figure S5. (a) − (c) TEM image of PtCu TRNs. (d) Histogram of the side length distribution of PtCu TRNs.

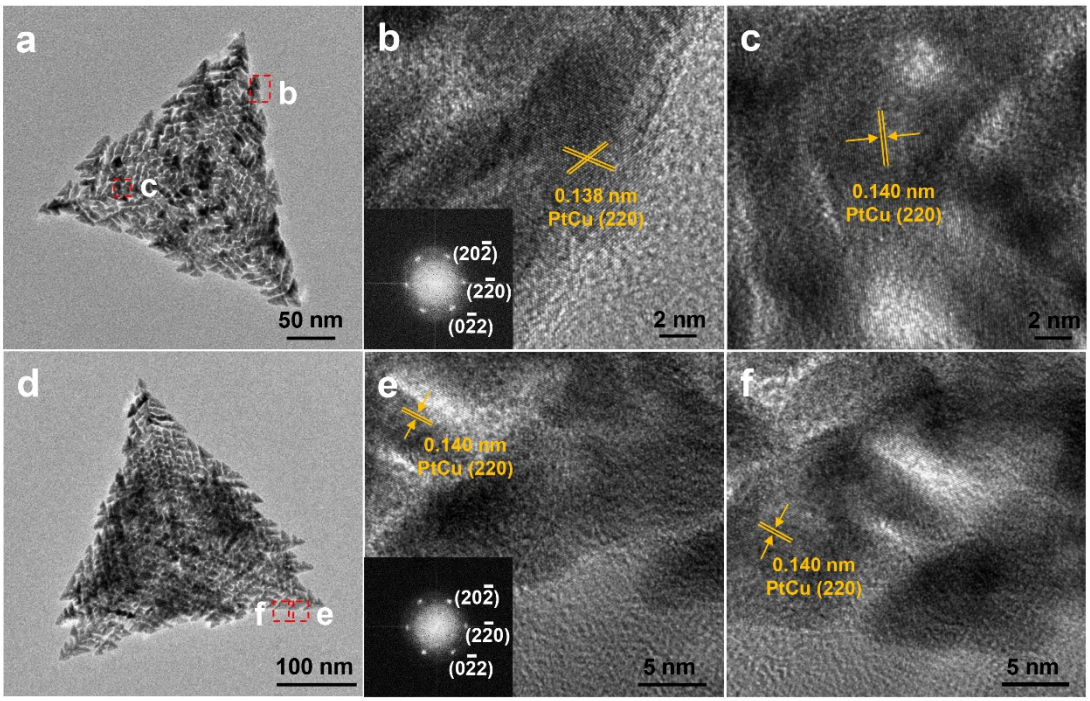

Figure S6. (a) and (d) TEM image of a single PtCu TRN. (b) and (c) The HRTEM images of the regions were marked in Figure a. The inset in Figure b showed the corresponding FFT image. (e) and (f) These were the HRTEM images of the regions marked in Figure d. The inset in Figure e showed the corresponding FFT image.

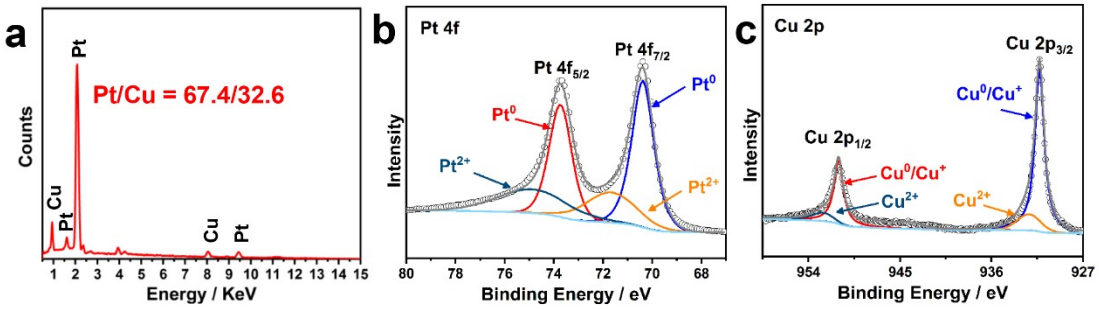

Figure S7. (a) SEM−EDS spectrum of PtCu TRNs. (b) and (c) Pt 4f and Cu 2p XPS spectra of PtCu TRNs.

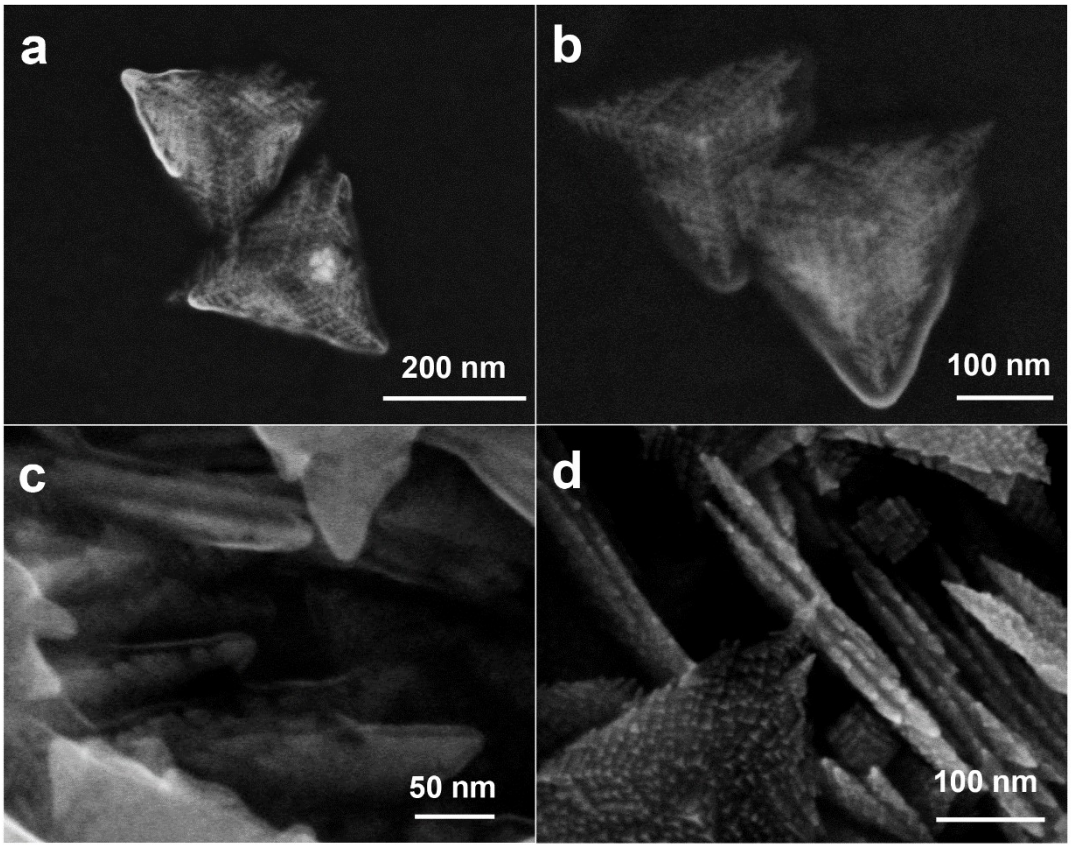

Figure S8. SEM images of PtCu TRNs.

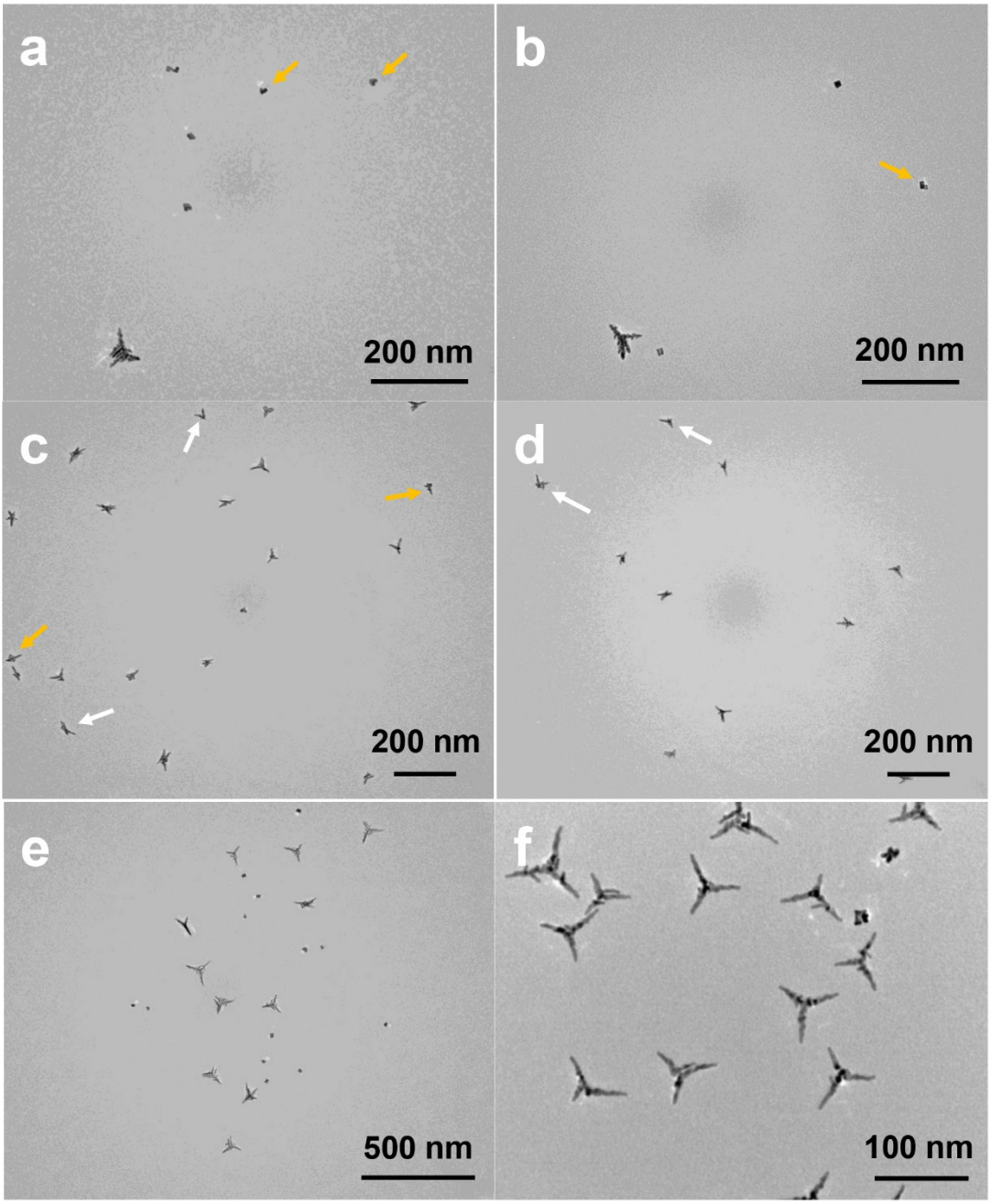

Figure S9. At different times, the SEM images of the product were obtained by the standard method of synthesizing PtCu TDNs. (a) and (b) 15 min. The arrow in the picture indicates the plate−like seed. (c) and (d) 30 min. The yellow arrow in the figure indicates the monopod, the white arrow indicates the bipod. (e) 1 h. (f) 2 h.

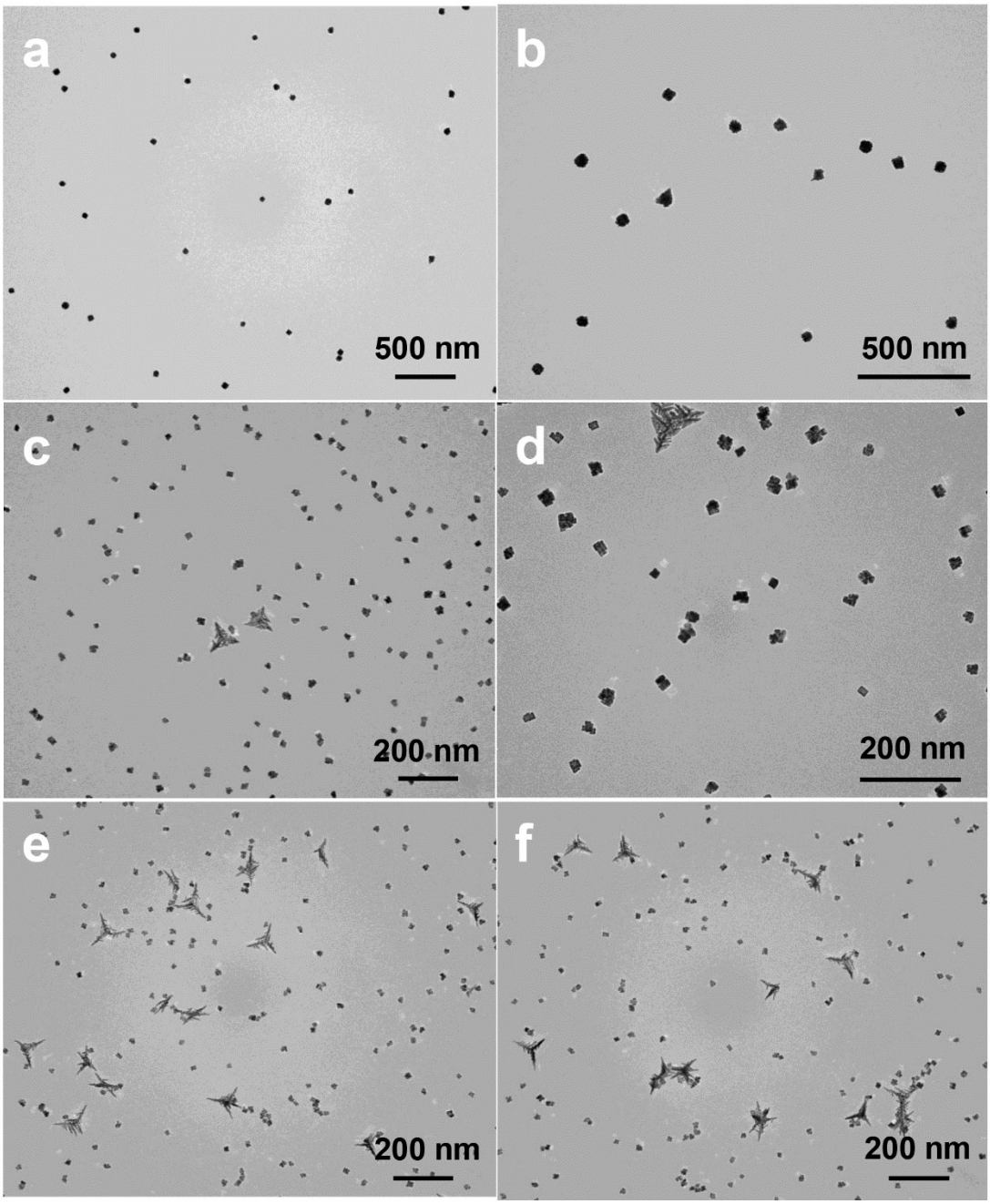

Figure S10. Under the standard procedure for the synthesis of PtCu TDNs, when the Pt/Cu content is different, the SEM image of the product. (a) and (b) Without Cu^{2+} ions. (c) and (d) $CuCl_2$ content is 1 mg. (e) and (f) $CuCl_2$ content is 7 mg.

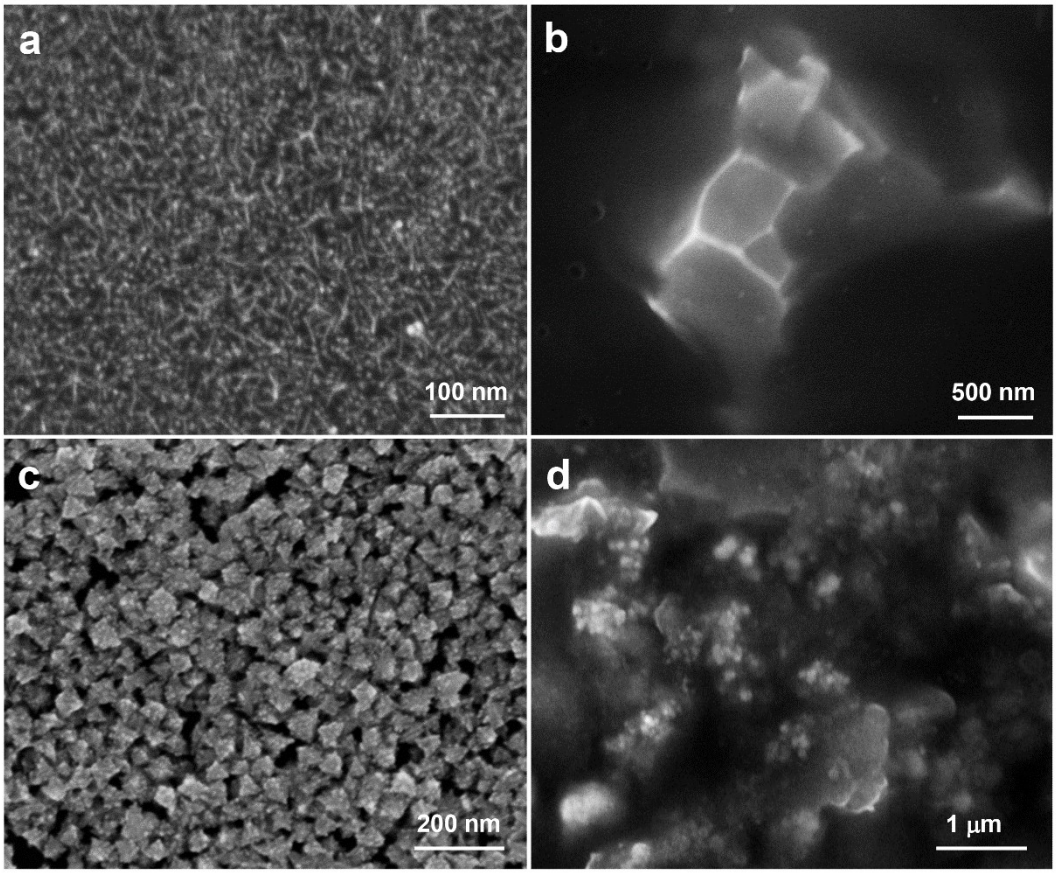

Figure S11. SEM images of PtCu TDNs obtained with standard procedures under different NaI content: (a) 400 and (b) 0 mg. (c) and (d) The SEM image of PtCu nanoparticles were collected from the reaction under the same conditions as PtCu TDNs synthesis, but NaI was replaced by KBr and KCl, respectively.

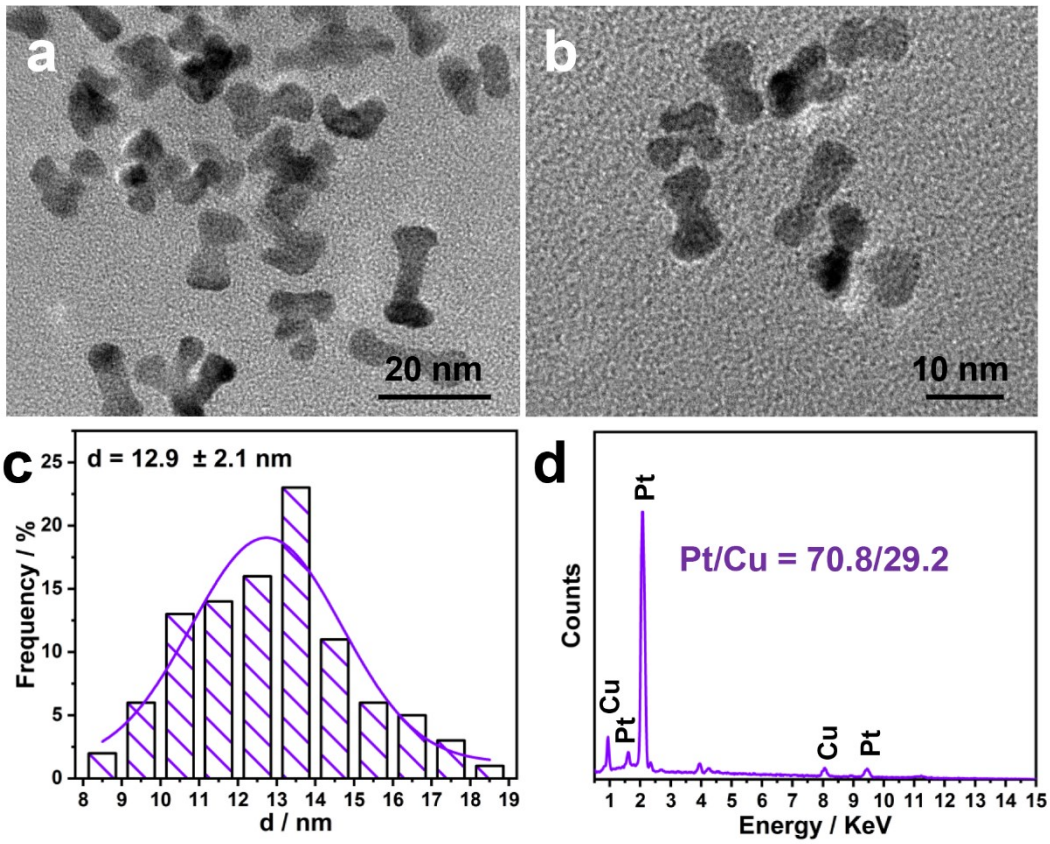

Figure S12. (a) and (b)TEM image of PtCu DLNs. (c) Histogram of the particle size distribution of PtCu DLNs. (d) SEM−EDS spectra of PtCu DLNs.

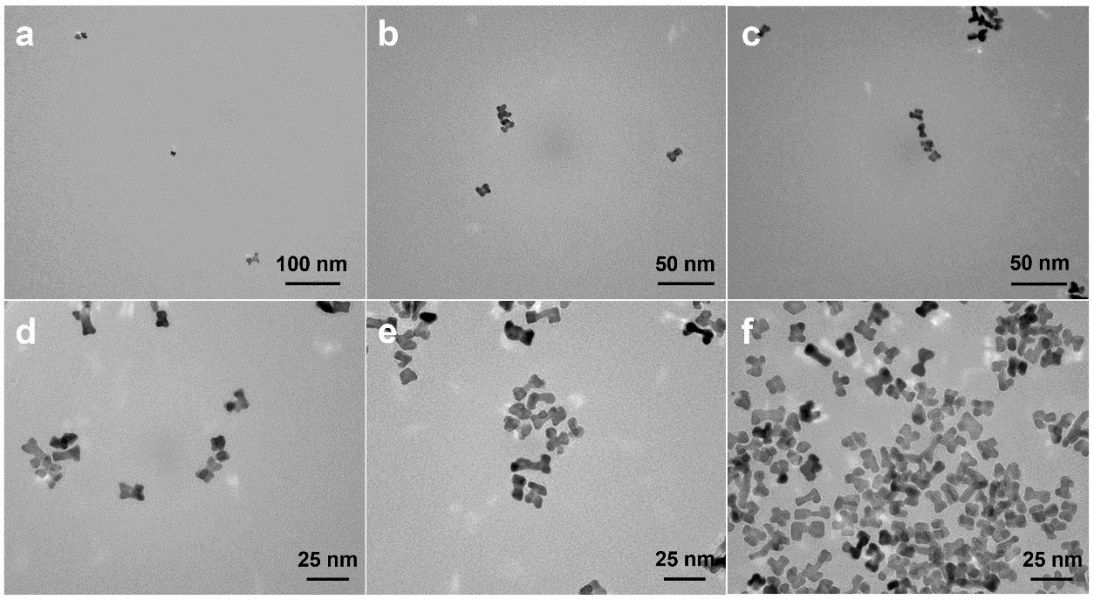

Figure S13. TEM images of the Pt−Cu HTBNFs at different reaction time points: (a) 30 min. (b) 1 h. (c) 2 h. (d) 3 h. (e) 4 h. (f) 5 h.

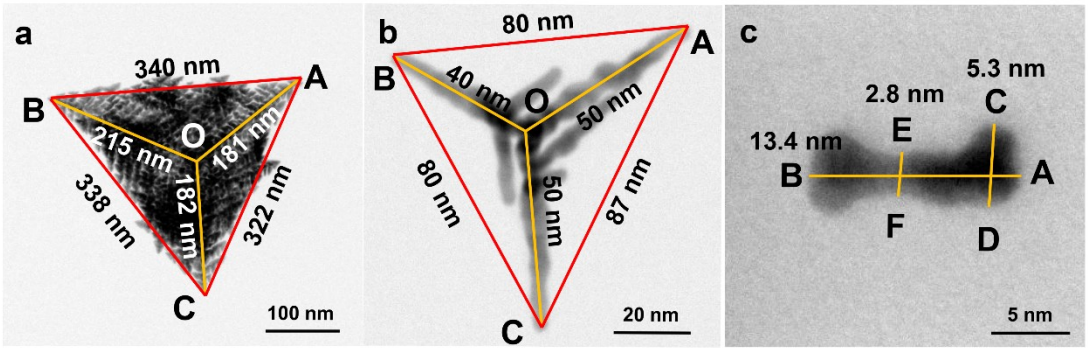

Figure S14. (a), (b) and (c) TEM of PtCu TRNs, TDNs and DLNs.

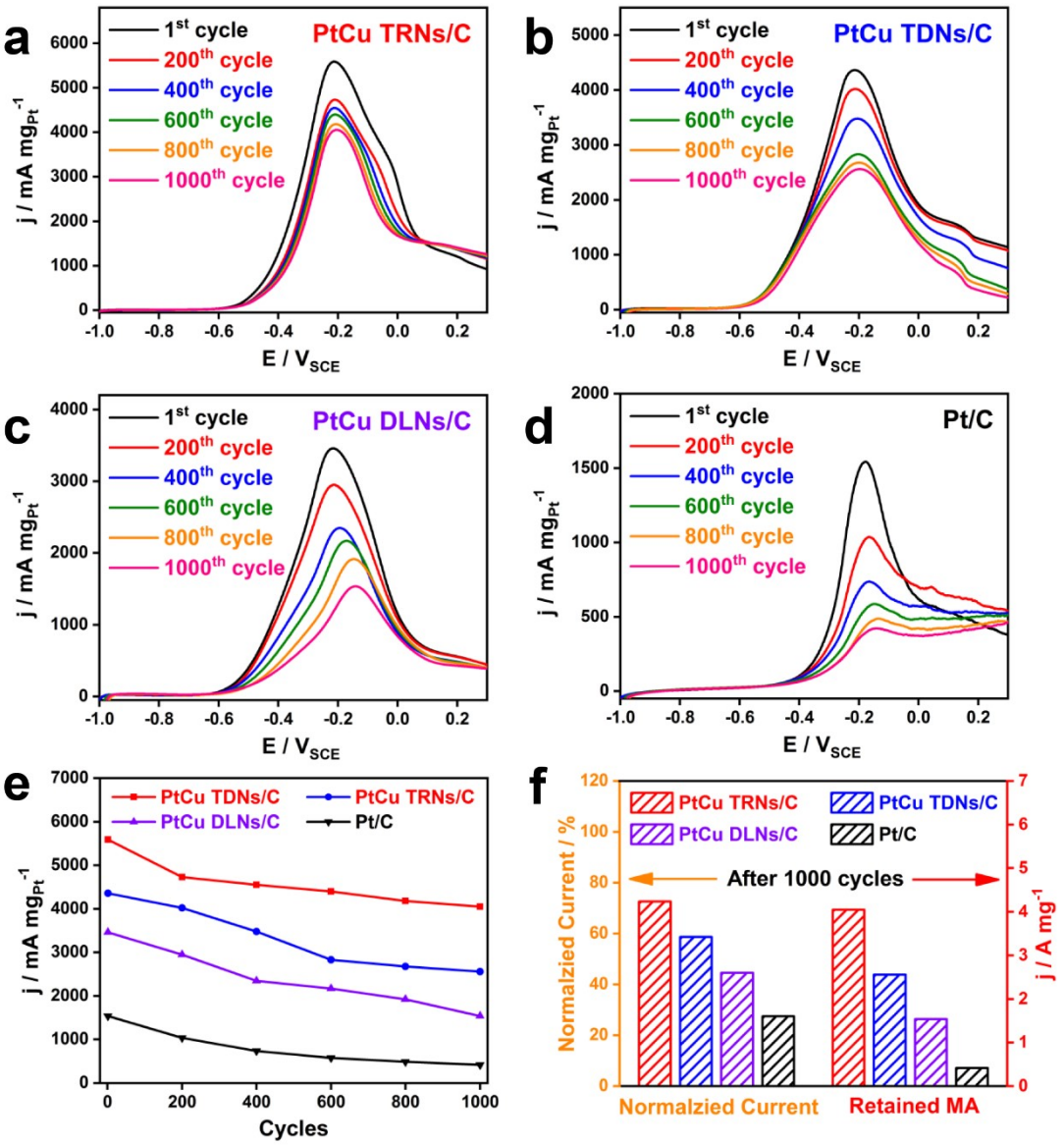

Figure S15. CVs (1st, 200 th, 400th, 600 th, 800 th and 1000 th cycle) of (a) the PtCu TRNs/C, (b) the PtCu TDNs, (c) the PtCu DLNs and (d) commercial Pt/C for EGOR, respectively. The potential was continuously scanned for 1000 sweeping cycles at 50 mV s^{-1} in 0.25 M KOH + 0.25 M EG for the EGOR durability test. (c) The change trend graph of the retained mass activity of different catalysts after 1000 cycles. (f) The normalized current and retained mass activity histogram of different catalysts after 1000 cycles.

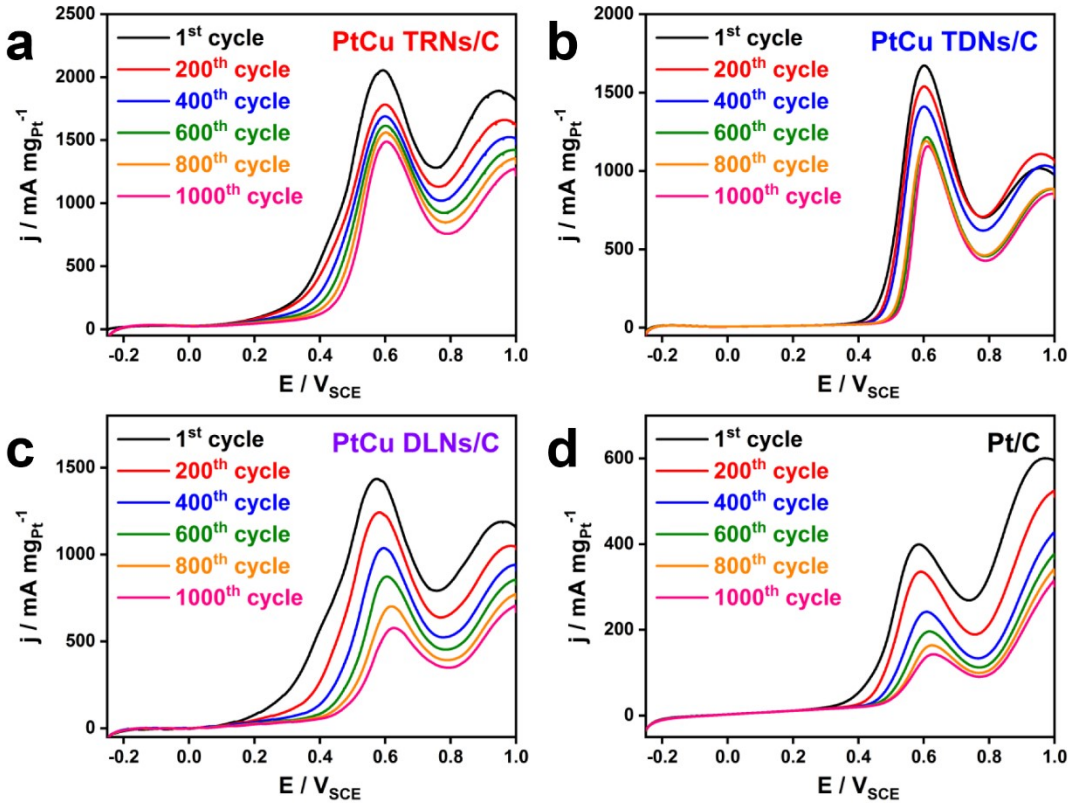

Figure S16. CVs (1st, 200 th, 400th, 600 th, 800 th and 1000 th cycle) of (a) the PtCu TRNs/C, (b) the PtCu TDNs, (c) the PtCu DLNs and (d) commercial Pt/C for EOR, respectively. The potential was continuously scanned for 1000 sweeping cycles at 50 mV s^{-1} in 0.1 M $HClO_4$ + 0.5 M ethanol for the EOR durability test.

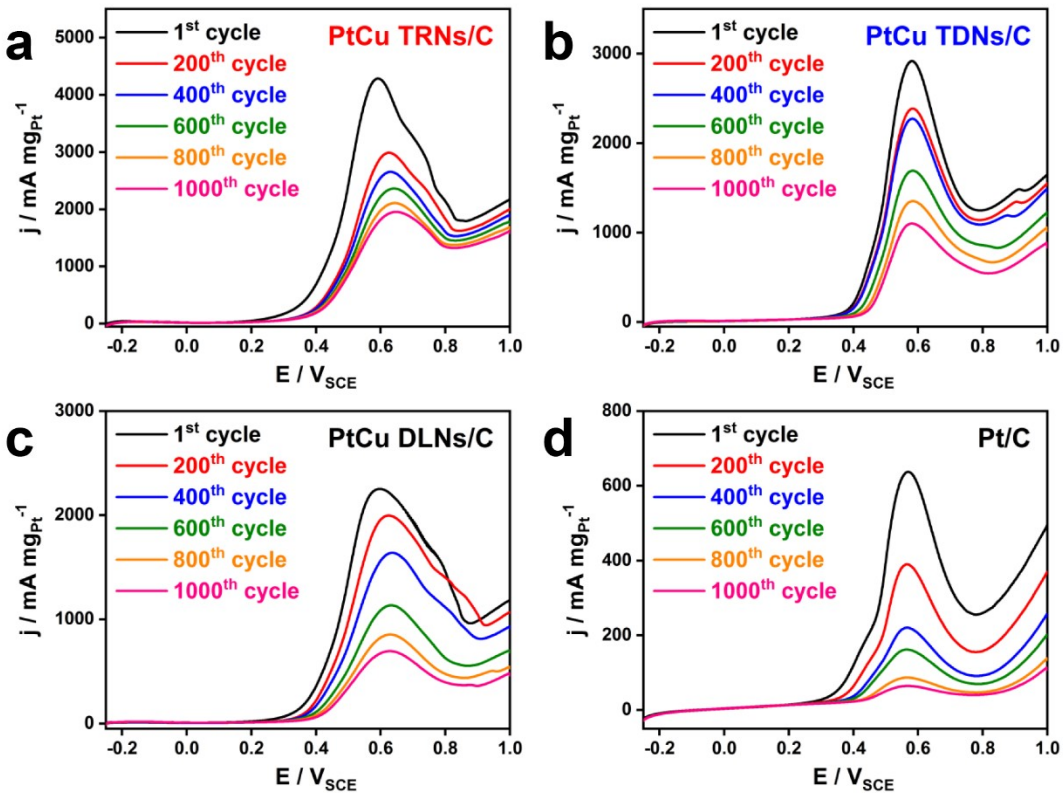

Figure S17. CVs (1st, 200 th, 400th, 600 th, 800 th and 1000 th cycle) of (a) the PtCu TRNs/C, (b) the PtCu TDNs, (c) the PtCu DLNs and (d) commercial Pt/C for MOR, respectively. The potential was continuously scanned for 1000 sweeping cycles at 50 mV s^{-1} in 0.1 M $HClO_4$ + 1.0 M methanol for the MOR durability test.

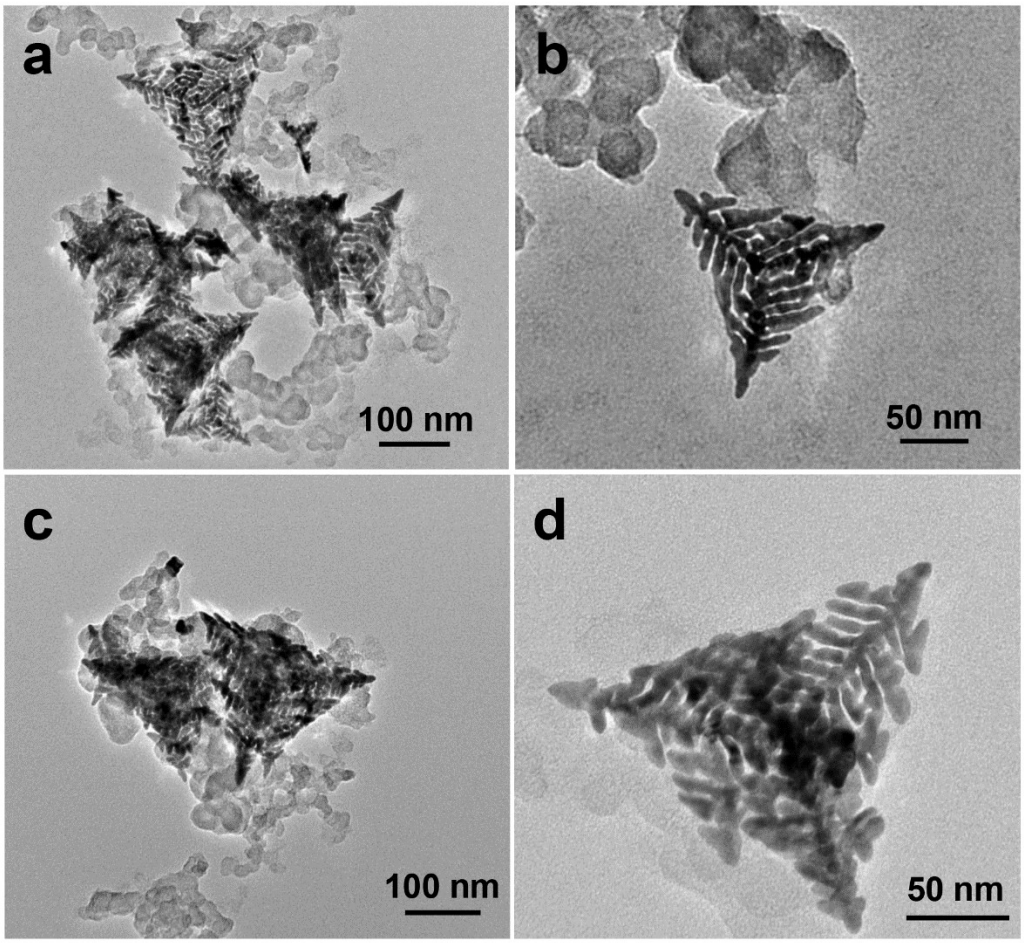

Figure S18. (a) and (b) TEM image of PtCu TRNs/C before alcohol oxidation test. (c) and (d) TEM image of PtCu TRNs/C after long−term alcohol oxidation test.

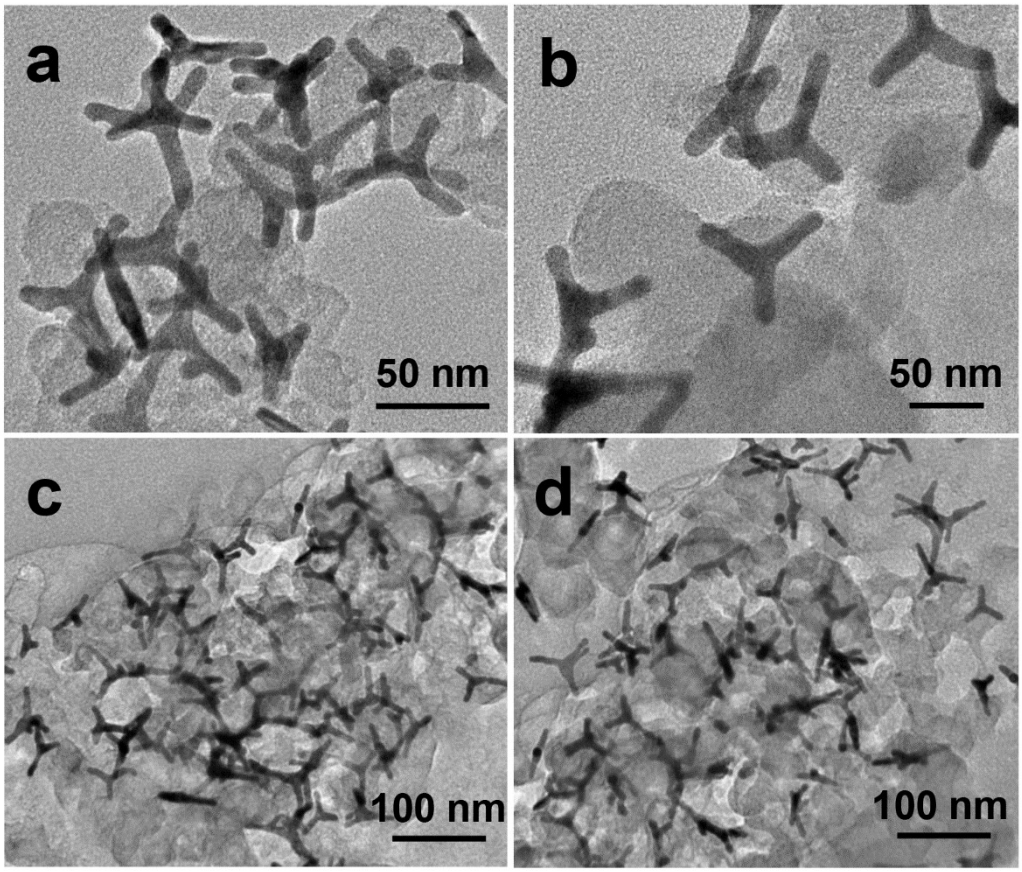

Figure S19. (a) and (b) TEM image of PtCu TDNs/C before alcohol oxidation test. (c) and (d) TEM image of PtCu TDNs/C after long−term alcohol oxidation test.

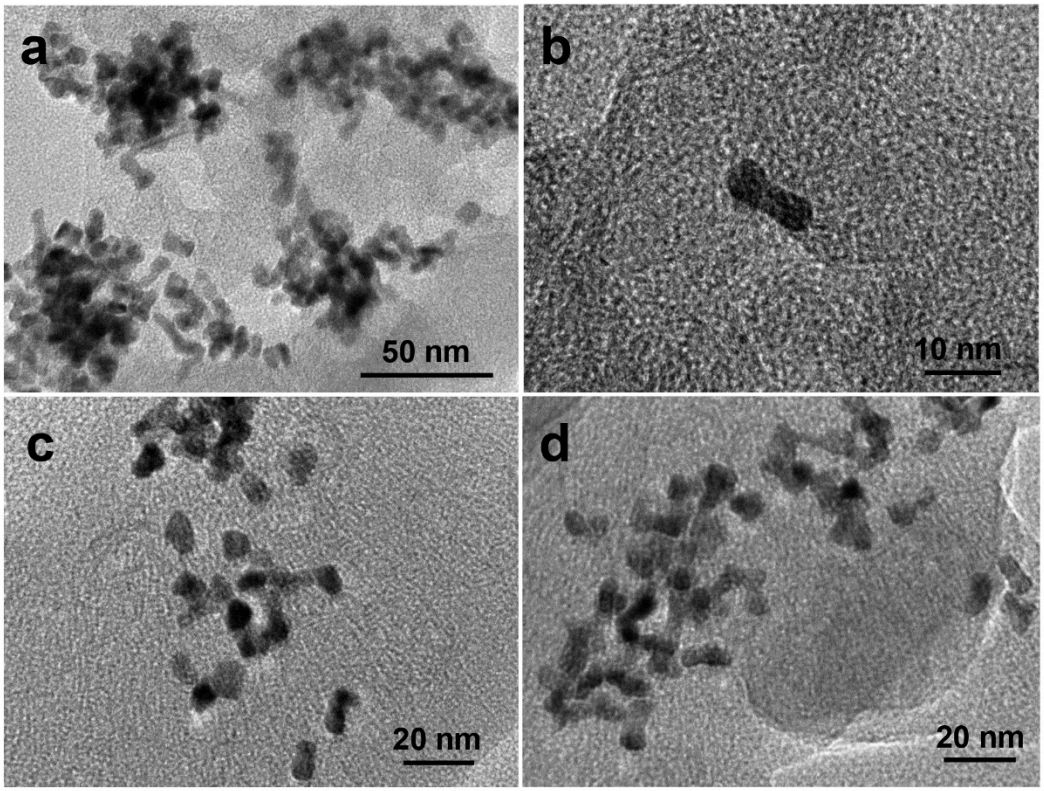

Figure S20. (a) and (b) TEM image of PtCu DLNs/C before alcohol oxidation test. (c) and (d) TEM image of PtCu DLNs/C after long−term alcohol oxidation test.

Table S1. EGOR performances of PtCu TRNs and various electrocatalysts from published works.

Catalyst	Specific activity /mA·cm^{-2}	Mass activity /A·mg^{-1}	Electrolyte	References
PtCu TRNs	11.6	5.8	0.25 M KOH+0.25 M $(CH_2OH)_2$	This Work
$Pt_{34}Pd_{33}Cu_{33}$	1.1	0.2	0.1 M $HClO_4$+0.5 M $(CH_2OH)_2$	[1]
$PtNi_{0.67}Pb_{0.23}$ NWs	0.7	0.4	0.1 M $HClO_4$+0.2 M $(CH_2OH)_2$	[2]
Pt_3Mn-Ru	1.3	0.2	0.1 M $HClO_4$+0.5 M $(CH_2OH)_2$	[3]
0.4%Mo/Pt_3Mn	1.2	0.2	0.1 M $HClO_4$+0.5 M $(CH_2OH)_2$	[4]
Pt_4Rh-S NCs	11.6	5.1	1.0 M KOH+1.0 M $(CH_2OH)_2$	[5]
$Pt_{52}Cu_{48}$ HTNCs	11.2	5.7	1.0 M KOH+1.0 M $(CH_2OH)_2$	[6]
Pt_3Cu NCs	9.7	5.2	1.0 M KOH+1.0 M $(CH_2OH)_2$	[7]
PtRhCo PAANFs	9.6	2.2	0.5 M KOH+0.5 M $(CH_2OH)_2$	[8]

Table S2. EOR performances of PtCu TRNs and various electrocatalysts from published works.

Catalyst	Specific activity /mA·cm^{-2}	Mass activity /A·mg^{-1}	Electrolyte	References
PtCu TRNs	4.2	2.1	0.1 M $HClO_4$+0.5 M CH_3CH_2OH	This Work
$Pt_{34}Pd_{33}Cu_{33}$	1.1	0.2	0.1 M $HClO_4$+0.5 M CH_3CH_2OH	[1]
$PtNi_{0.67}Pb_{0.23}$ NWs	1.1	0.8	0.1 M $HClO_4$+0.2 M CH_3CH_2OH	[2]
$PtCu_{2.1}$ NWs	2.2	1.0	0.1 M $HClO_4$+0.2 M CH_3CH_2OH	[9]
PtCu nanostars	4.5	0.6	0.5 M H_2SO_4+2.0 M CH_3CH_2OH	[10]
Pt_1Ru_1/C	–	0.8	0.5 M H_2SO_4+0.5 M CH_3CH_2OH	[11]
porous Pt−$Bi(OH)_3$	–	0.6	0.5 M H_2SO_4+0.5 M CH_3CH_2OH	[12]
$Pt_3Ru/Ti_{0.7}W_{0.3}O_2$	–	0.3	0.5 M H_2SO_4+0.5 M CH_3CH_2OH	[13]
Pd@PtRh nanorings	4.2	–	0.5 M NaOH+0.5 M CH_3CH_2OH	[14]

Table S3. MOR performances of PtCu TRNs and various electrocatalysts from published works.

Catalyst	Specific activity /mA·cm^{-2}	Mass activity /A·mg^{-1}	Electrolyte	References
PtCu TRNs	8.5	4.2	0.1 M $HClO_4$+1.0 M CH_3OH	This Work
$Pt_{34}Pd_{33}Cu_{33}$	4.2	0.7	0.1 M $HClO_4$+0.5 M CH_3OH	[1]
$PtNi_{0.67}Pb_{0.23}$ NWs	3.1	2.4	0.1 M $HClO_4$+0.2 M CH_3OH	[2]
$PtCu_{2.1}$ NWs	3.3	1.6	0.1 M $HClO_4$+0.2 M CH_3OH	[9]
$Pt_1Ru_{0.5}$/C@NC	5.3	–	0.1 M $HClO_4$+1.0 M CH_3OH	[15]
r–$Pt_{0.75}$Cu/C	5.2	2.2	0.5 M H_2SO_4+1.0 M CH_3OH	[16]
PtCu nanostars	3.5	0.6	0.5 M H_2SO_4+1.0 M CH_3OH	[10]
PtMo nanowires	2.1	1.0	0.1 M $HClO_4$+1.0 M CH_3OH	[17]
Cu@Pt/C	2.1	0.5	0.1 M $HClO_4$+0.1 M CH_3OH	[18]

References:

1. Lan, J.; Wang, K.; Yuan, Q.; Wang, X., Composition−controllable synthesis of defect−rich PtPdCu nanoalloys with hollow cavities as superior electrocatalysts for alcohol oxidation. *Mater Chem Front* **2017,** *1* (6), 1217−1222.

2. Zhang, N.; Zhu, Y. M.; Shao, Q.; Zhu, X.; Huang, X. Q., Ternary PtNi/PtxPb/Ptcore/multishell nanowires as efficient and stable electrocatalysts for fuel cell reactions. *J Mater Chem A* **2017,** *5* (36), 18977−18983.

3. Wang, Y.; Zheng, M.; Sun, H.; Zhan, X.; Luan, C. L.; Li, Y. R.; Zhao, L.; Zhao, H. H.; Dai, X. P.; Ye, J. Y.; Wang, H.; Sun, S. G., Catalytic Ru containing Pt3Mn nanocrystals enclosed with high−indexed facets: Surface alloyed Ru makes Pt more active than Ru particles for ethylene glycol oxidation. *Appl Catal B−Environ* **2019,** *253*, 11−20.

4. Wang, Y.; Zhuo, H. Y.; Sun, H.; Zhang, X.; Dai, X. P.; Luan, C. L.; Qin, C. L.; Zhao, H. H.; Li, J.; Wang, M. L.; Ye, J. Y.; Sun, S. G., Implanting Mo Atoms into Surface Lattice of Pt3Mn Alloys Enclosed by High−Indexed Facets: Promoting Highly Active Sites for Ethylene Glycol Oxidation. *Acs Catal* **2019,** *9* (1), 442−455.

5. Gao, F.; Zhang, Y. P.; Song, P. P.; Wang, J.; Song, T. X.; Wang, C.; Song, L.; Shiraishi, Y.; Du, Y. K., Precursor−mediated size tuning of monodisperse PtRh nanocubes as efficient electrocatalysts for ethylene glycol oxidation. *J Mater Chem A* **2019,** *7* (13), 7891−7896.

6. Xu, H.; Song, P. P.; Gao, F.; Shiraishi, Y.; Du, Y. K., Hierarchical branched platinum−copper tripods as highly active and stable catalysts. *Nanoscale* **2018,** *10* (17), 8246−8252.

7. Xu, H.; Liu, C. F.; Song, P. P.; Wang, J.; Gao, F.; Zhang, Y. P.; Shiraishi, Y.; Di, J. W.; Du, Y. K., Ethylene Glycol Electrooxidation Based on Pentangle−Like PtCu Nanocatalysts. *Chem−Asian J* **2018,** *13* (6), 626−630.

8. Chen, Y.; Zheng, X. X.; Huang, X. Y.; Wang, A. J.; Zhang, Q. L.; Huang, H.; Feng, J. J., Trimetallic PtRhCo petal−assembled alloyed nanoflowers as efficient and stable bifunctional electrocatalyst for ethylene glycol oxidation and hydrogen evolution reactions. *J Colloid Interf Sci* **2020,** *559*, 206−214.

9. Zhang, N.; Bu, L. Z.; Guo, S. J.; Guo, J.; Huang, X. Q., Screw Thread−Like Platinum−Copper Nanowires Bounded with High Index Facets for Efficient Electrocatalysis. *Nano Lett* **2016,** *16* (8), 5037−5043.

10. Huang, L. P.; Zhang, W.; Li, P.; Song, Y. B.; Sheng, H. T.; Du, Y. X.; Wang, Y. G.; Wu, Y. E.; Hong, X.; Ding, Y. H.; Yuan, X. Y.; Zhu, M. Z., Exposing Cu−Rich {110} Active Facets in PtCu nanostars for boosting electrochemical performance toward multiple liquid fuels electrooxidation. *Nano Res* **2019,** *12* (5), 1147−1153.

11. Hu, Y. M.; Zhu, A. M.; Zhang, Q. G.; Liu, Q. L., Preparation of PtRu/C core−shell catalyst with polyol method for alcohol oxidation. *Int J Hydrogen Energ* **2016,** *41* (26), 11359−11368.

12. Yuan, X. L.; Jiang, B.; Cao, M. H.; Zhang, C. Y.; Liu, X. Z.; Zhang, Q. H.; Lyu, F. L.; Gu, L.; Zhang, Q., Porous Pt nanoframes decorated with Bi(OH)(3) as highly efficient and stable electrocatalyst for ethanol oxidation reaction. *Nano Res* **2020,** *13* (1), 265−272.

13. Pham, H. Q.; Huynh, T. T.; Pham, T. M.; Ho, V. T. T., Boosting alcohol electro−oxidation reaction with bimetallic PtRu nanoalloys supported on robust Ti0.7W0.3O2 nanomaterial in direct liquid fuel cells. *Int J Hydrogen Energ* **2021,** *46* (31), 16776−16786.

14. Zou, J. S.; Wu, M.; Ning, S. L.; Huang, L.; Kang, X. W.; Chen, S. W., Ru@Pt Core−Shell Nanoparticles: Impact of the Atomic Ordering of the Ru Metal Core on the Electrocatalytic Activity of the Pt Shell. *Acs Sustain Chem Eng* **2019,** *7* (9), 9007−9016.

15. Wang, Q. M.; Chen, S. G.; Jiang, J.; Liu, J. X.; Deng, J. H.; Ping, X. Y.; Wei, Z. D., Manipulating the surface composition of Pt−Ru bimetallic nanoparticles to control the methanol oxidation reaction pathway. *Chem Commun* **2020,** *56* (16), 2419−2422.

16. Shi, Y.; Fang, Y.; Zhang, G. L.; Wang, X. S.; Cui, P.; Wang, Q.; Wang, Y. X., Hollow PtCu nanorings with high performance for the methanol oxidation reaction and their enhanced durability by using trace Ir. *J Mater Chem A* **2020,** *8* (7), 3795−3802.

17. Lu, S. L.; Eid, K.; Lin, M.; Wang, L.; Wang, H. J.; Gu, H. W., Hydrogen gas−assisted synthesis of worm−like PtMo wavy nanowires as efficient catalysts for the methanol oxidation reaction. *J Mater Chem A* **2016,** *4* (27), 10508−10513.

18. Polani, S.; Shviro, M.; Shokhen, V.; Zysler, M.; Glusen, A.; Dunin−Borkowski, R.; Carmo, M.; Zitoun, D., Size dependent oxygen reduction and methanol oxidation reactions: catalytic activities of PtCu octahedral nanocrystals. *Catal Sci Technol* **2020,** *10* (16), 5501−5512.